mass-to-charge ratios appear from left to right (decreasing cyclotron frequencies ω_2). As may be expected, only the ions CHD_2^+, CD_3^+, and $CHD_3^{\bullet+}$ give rise to signals on the line of primary ions. Dotted lines with arrows indicate how the t_1 modulation (ω_1 frequency) is carried from the primary ions to the secondary ions. The ions $CH_2D_3^+$ and CHD_4^+ appear only as daughters of $CHD_3^{\bullet+}$. The heavier ions $C_2HD_4^+$ are produced from collisions involving either CHD_2^+ or CD_3^+. The species $C_2H_2D_3^+$ only appears as daughter of CHD_2^+, while $C_2D_5^+$ stems only from CD_3^+. All these processes can be evaluated from a single 2D spectrum.

Further Experiments

Two-dimensional FT-ICR can be combined with a variety of perturbations. In particular, it is possible to admit a pulse of a neutral reacting gas to the cell in the course of the reaction interval τ_m of the 2D FT-ICR sequence. A preliminary experiment has shown that this is indeed feasible. The first two rf pulses were applied while the cell contained only argon ions Ar^+. In the reaction interval τ_m, a pulse of CH_4 gas was introduced into the cell. No further ionization pulses were applied however. In the 2D spectrum, clear evidence was found for secondary ions CH_3^+ and even for tertiary ions $C_2H_5^+$, both t_1 modulated at the frequency of the Ar^+ ions. Clearly, the transfer of the modulation from one species to another provides evidence for the reactions $Ar^+ + 2CH_4 \rightarrow Ar + CH_3^+ + H^\bullet + CH_4 \rightarrow Ar + C_2H_5^+ +$ neutrals.

Further work is in progress to explore the effects of laser pulses applied to the ions in the course of the reaction interval τ_m of the experiment. Such techniques open new perspectives for studying very complex reaction networks.

As mentioned above, the third pulse is normally chirped, so that the ω_2 domain may extend over a large bandwidth. In some cases however, it may be of interest to use very high resolution in the ω_2 domain in order to distinguish reaction products that have similar mass-to-charge ratios. We have carried out two-dimensional experiments where the first two pulses were chirped, while the third pulse was derived from a monochromatic rf carrier. The signal was observed with heterodyne detection to obtain high-resolution spectra in the ω_2 domain. This allowed us to distinguish the product ions $CH_3D^{\bullet+}$ and CH_5^+, in order to identify the parent ions from which they originated. It does not seem worthwhile to provide illustrations of such spectra, for their general appearance is very similar to Figure 5.

Experimental Section

The spectra were obtained with a Spectrospin CMS-47 FT-ICR spectrometer equipped with a 3 T superconducting magnet and an Aspect 3000 computer system. Methane (CH_4 and CD_3H, respectively) at 6.10^{-8} mbar was ionized with 20-ms pulses of 70-eV electrons. Other experimental conditions are given in the captions.

Conclusions

We have shown that two-dimensional FT-ICR spectra can be obtained with frequency-swept pulses in order to overcome bandwidth limitations. Broad-band 2D FT-ICR appears to develop into a promising tool for investigating ion–molecule reactions and other processes such as photofragmentation. Frequency-swept pulses may also be useful in other applications of two-dimensional spectroscopy, such as in ESR spectra[8,9] and in rotational microwave spectra.[10] Whether two-dimensional techniques will prove to be competitive with traditional ion-ejection methods,[2,3] or with more elaborate schemes based on ion ejection such as the Hadamard method,[15] remains to be seen. Experience in NMR spectroscopy has shown that the appreciation of the relative merits of one- and two-dimensional spectroscopy may fluctuate as a result of the discovery of new methods and applications.[6]

Acknowledgment. We are indebted to A. G. Marshall, F. W. McLafferty and M. L. Gross for helpful comments. This research was supported in part by the Swiss National Science Foundation and by a grant from Spectrospin AG (Fällanden, Switzerland).

(15) McLafferty, F. W.; Stauffer, D. B.; Loh, S. Y.; Williams, E. R. *Anal. Chem.* **1987**, *59*, 2212.

Unusual Spectroscopic Features in the Emission and Absorption Spectra of Single-Crystal $K_2[PtCl_4]$ Caused by Multiple-Mode Excited-State Distortions

D. M. Preston,[†] Wolfgang Güntner,[‡] Alfred Lechner,[‡] Günter Gliemann,*[,‡] and Jeffrey I. Zink*[,†]

Contribution from the Department of Chemistry and Biochemistry, University of California, Los Angeles, California 90024-1569, and Institut für Physikalische und Theoretische Chemie, University of Regensburg, 8400 Regensburg, FRG. *Received January 7, 1988*

Abstract: Two unusual features are observed in the electronic emission and absorption spectra of single-crystal $K_2[PtCl_4]$. First, a regularly spaced vibronic progression of 315 cm^{-1} is observed in the luminescence spectrum which does not correspond to any normal vibrational modes of the molecule bound in the crystal. The spectrum is interpreted in terms of the missing mode effect (MIME). Calculations of the contributing vibrations and excited-state distortions are presented. Both the time-dependent theory and the eigenstate explanation are discussed. Second, a 1800-cm^{-1} gap between the emission and absorption spectrum is found in which no measurable emission intensity or absorption intensity is observed. This energy gap is explained in terms of the intramolecular distortion along the non-totally symmetric mode which is required by the MIME. The magnitude of the energy gap is calculated from the distortion along this mode. The unmeasurable low vibronic intensities in the gap are explained by using the time-dependent theory of electronic spectroscopy.

The electronic emission and absorption spectra of the tetrachloroplatinate(II) ion and its derivatives are continuing to receive detailed attention.[1-6] In spite of the high symmetry and the apparent simplicity of the square-planar $PtCl_4^{2-}$, the electronic spectra and the electronic structure contain a number of interesting features.

[†] University of California, Los Angeles.
[‡] University of Regensburg.

(1) Martin, D. S.; Lenhardt, C. A. *Inorg. Chem.* **1964**, *3*, 1368.
(2) Martin, D. S.; Tucker, M. A.; Kassman, A. J. *Inorg. Chem.* **1965**, *4*, 1682.

0002-7863/88/1510-5628$01.50/0

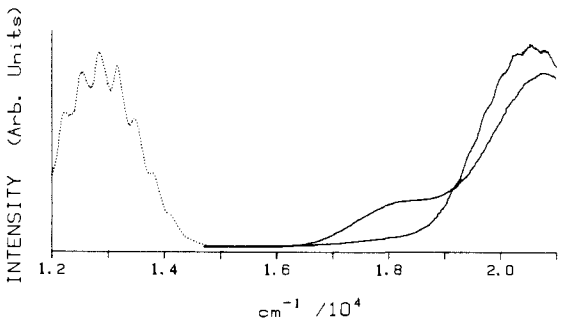

Figure 1. Single-crystal polarized emission (···) and absorption (—) spectra of $K_2[PtCl_4]$. The absorption spectra were taken in E||c and E⊥c polarization on a 450 μm thick crystal at 10 K. The emission spectrum was taken in E||c polarization at 10 K.

As part of our interest in this system, we have obtained single-crystal luminescence spectra at low temperature containing high resolution of the vibronic structure and absorption spectra from both thick and thin single crystals to examine the low-energy range. Two unusual features of these spectra were uncovered. First, the emission spectrum contains a regularly spaced series of vibronic bands whose energy spacing does not correspond to any normal vibrational mode of the molecule bound in the crystal. This absence of a normal mode of the required frequency, the missing mode effect or MIME, has been recognized and analyzed in other molecules.[7-9] It is a consequence of two or more displaced normal modes. However, the D_{4h} $PtCl_4^{2-}$ ion has only one totally symmetric normal mode. Second, the emission and absorption spectra reveal a large (~1800 cm^{-1}) region in which no emission intensity nor absorption is found.

In this paper, the vibronic structure of the luminescence spectrum and the energy gap between the emission and absorption spectra are analyzed. It is shown that both of these unusual spectroscopic features can be explained in terms of a configurational displacement of the molecule in its lowest energy excited state relative to its ground electronic state along both a totally symmetric and a non-totally symmetric mode. The MIME is analyzed and the distortions are calculated. The magnitude of the energy gap is calculated, and the absence of observable intensity in the gap is explained.

Experimental Section

$K_2[PtCl_4]$. The compound was prepared according to the literature method.[10]

Absorption Spectra. Thin (about 30 μm) and thick (about 450 μm) single crystals of $K_2[PtCl_4]$ were grown between quartz plates, and the low-temperature polarized spectra were taken at 8 K on a spectrometer that has been previously described.[4,11] Thicker (~1.5 mm) crystals were used to carefully examine the absorption between 22000 and 14000 cm^{-1}.

Emission Spectra. Oriented single crystals of $K_2[PtCl_4]$ were cooled to 10 K in a helium cryostat, and the emission spectrum was taken with the *c* axis of the crystal (which is parallel to the symmetry axis of the $[PtCl_4]^{2-}$ ion) perpendicular to the direction of observation. The 457-nm line of an Ar ion laser was used to excite the sample. The instruments have been previously described.[11] Only the ambient pressure spectrum was used in this study.

Raman Spectra. Both single-crystal and powder Raman spectra were taken at room temperature with use of the 514.5-nm line of an Ar ion laser and the 632.8-nm line of a helium–neon laser. A triple monochromator and a diode-array detector interfaced to its own computer were used to collect, store, and display the spectra.

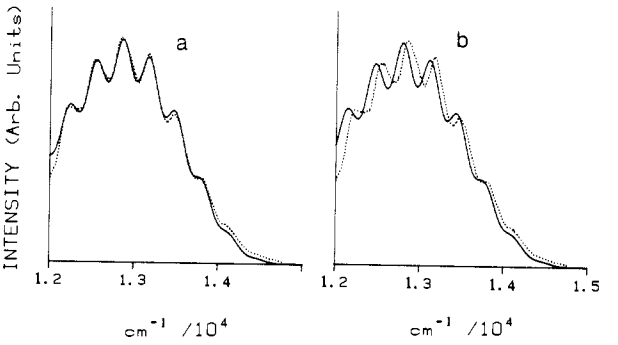

Figure 2. Experimental (···) and calculated (—) emission spectra of $K_2[PtCl_4]$. Experimental conditions: single crystal, 10 K, E||c polarization. Calculation parameters: (a) two modes: A_{1g}, 329 cm^{-1}, Δ = 2.25; B_{1g}, 304 cm^{-1}8 Δ = 2.58 E_{00} = 14425 5cm^{-1}; (b) one mode, A_{1g}, 329 cm^{-1}, Δ = 3.42, E_{00} = 14425 cm^{-1}. Both plots were calculated with Γ = 87 cm^{-1}.

Table I. Positions of the Peaks in the Emission Spectrum of $K_2[PtCl_4]$[a]

position, cm^{-1}	difference, cm^{-1}
14435	
	320
14115	
	315
13800	
	320
13480	
	310
13170	
	320
12850	
	310
12540	
	310
12230	
	average 315 ± 5

[a] See Figure 2.

Results

1. Electronic Spectra. The general features of the emission and low-energy absorption spectra of single-crystal $K_2[PtCl_4]$ are shown in Figure 1. All spectra are corrected for instrument response. The emission spectrum peaks at 12850 cm^{-1} and contains moderately well resolved vibronic structure. The vibronic peaks are regularly spaced and separated by 315 ± 5 cm^{-1}. The low-energy region of the E||c polarized absorption spectrum of a single crystal with a thickness of about 450 μm contains a weak structureless shoulder at about 17600 cm^{-1} and a distinctly structured peak at 20550 cm^{-1}. The E⊥c polarized absorption spectrum consists of a weak peak at 18000 cm^{-1} with barely discernible vibronic structure and a smooth peak at 20950 cm^{-1}. The Stokes shift between the lowest energy absorption band and the emission band is 4750 cm^{-1}

Detailed features of the emission spectrum are shown in Figure 2. The highest energy vibronic peak that can be detected is at 14435 cm^{-1}. The vibronic peaks disappear when the crystals are warmed to about 70 K. Varying the temperature did not cause any measureable change in the positions or the relative intensities of the vibronic peaks. The energies of each of the vibronic peaks in Figure 2 are tabulated in Table I.

The absorption spectra shown in Figure 1 are taken from relatively thick crystals in order to examine the low-energy features. Two bands are clearly revealed as shown in Figure 1. A weak feature in this region was observed also in the spectrum of $[PtCl_4]^{2-}$ doped in cesium hexachlorozirconate.[3] Ligand field calculations place the $\Gamma_1(^3E_g,^3A_{2g})$ transition at this energy.[6] In spectra of thinner crystals (~30 μm) the higher energy features with much larger molar absorptivities are on scale. These features

(3) Patterson, H. H.; Godfrey, J. J.; Khan, S. M. *Inorg. Chem.* **1972**, *11*, 2872.
(4) Tuszynski, W.; Gliemann, G. *Z. Naturforsch, A* **1979**, *34A*, 211.
(5) Yersin, H.; Otto, H.; Zink, J. I.; Gliemann, G. *J. Am. Chem. Soc.* **1980**, *102*, 951.
(6) Vanquickenborne, L. G.; Ceulemans, A. *Inorg. Chem.* **1981**, *20*, 796.
(7) Tutt, L.; Tannor, D.; Heller, E. J.; Zink, J. I. *Inorg. Chem.* **1982**, *21*, 3859.
(8) Tutt, L.; Tannor, D.; Schindler, J. W.; Heller, E. J.; Zink, J. I. *J. Phys. Chem.* **1983**, *87*, 3017.
(9) Tutt, L.; Zink, J. I. *J. Am. Chem. Soc.* **1986**, *108*, 5830.
(10) Brauer, G. *Handbuch der* präparativen *anorganischen Chemie*; F. Enke: Stuttgart, 1962.
(11) Yersin, H.; Gliemann, G. *Messtechnik* **1972**, *80*, 99.

Table II. Vibrational Frequencies for Solid K_2PtCl_4

symmetry	freq, cm^{-1}	ref
A_{2u}	168	*a*
	170	*b*
E_u	191	*a*
	190	*b*
B_{2g}	195	*c*
	194	*d*
B_{1g}	304	*c*
	302	*d*
E_u	321	*a*
	325	*b*
A_{1g}	329	*c*
	329	*d*

[a] Hendra, P. J. *J. Chem. Soc. A* **1966**, 1298. [b] Hiraishi, J.; Shimanouchi, T. *Spectrochim. Acta* **1966**, *22*, 1483. [c] This work. [d] Hendra, P. J. *Spectrochim. Acta* **1967**, *23A*, 2871.

have been extensively discussed previously.[4,6]

The spectra in Figure 1 reveal a region between the onset of the emission and the absorption bands where there is no observable emission or absorption intensity. A careful search for emission intensity at energies higher than 14 435 cm^{-1} did not reveal any additional bands. Likewise, careful examination of the absorption spectra of thick crystals (~1.5 mm) did not reveal any measurable absorbance at energies lower than about 16 200 cm^{-1}. There is a 1800-cm^{-1} energy gap between the onsets of the emission and absorption bands.

2. Vibrational Spectra. The normal vibrational modes and the vibrational frequencies of solid $K_2[PtCl_4]$ are given in Table II. Care was taken in these measurements because $K_2[PtCl_6]$, a common impurity in $K_2[PtCl_4]$, contains strong bands at about 170, 320, and 350 cm^{-1} which may be mistaken for the weaker 195, 304, and 329-cm^{-1} bands of the square-planar complex.

Discussion

1. The Missing Mode Effect. The average spacing in the vibronic progression of the experimental emission spectrum is 315 ± 5 cm^{-1}. This frequency does not match the frequency of the totally symmetric mode, 329 cm^{-1}, and in fact does not match that of any normal mode in $K_2[PtCl_4]$ (Table II). The modes that are closest in frequency to the emission spacing are the B_{1g} mode (304 cm^{-1}), the E_u mode (325 cm^{-1}),[12] and the A_{1g} mode (329 cm^{-1}). The latter is the only totally symmetric normal mode in this complex.

An attempt to fit the experimental emission spectrum by using a distortion in only the totally symmetric mode is shown in Figure 2b. The calculated intensities fit the intensities in the experimental spectrum. However, the spacings between the peaks in the progression do not match. The separation between the calculated and observed energies becomes progressively larger as the vibrational quantum number increases. The origin for both spectra is at 14 435 cm^{-1}. By the seventh peak of the A_{1g} progression, the calculated (12 451 cm^{-1}) and experimental peaks (12 535 cm^{-1}) differ by about 84 cm^{-1}. Thus, the progression in the emission spectrum of $K_2[PtCl_4]$ is not caused by a distortion in only the totally symmetric mode.

The best two-mode fit to the experimental emission spectrum of $K_2[PtCl_4]$ with use of the frequencies from Table II is shown in Figure 2a. In the best-fit calculated emission spectrum, the A_{1g} mode (329 cm^{-1}) and the B_{1g} mode (304 cm^{-1}) combine to produce the MIME frequency in the main progression. No other vibrational mode was found that could combine with the A_{1g} mode to produce the spacing of 315 cm^{-1}. Very small contributions from other modes are possible, but they only serve to decrease the resolution of the vibronic structure and do not improve the fit.

A detailed discussion of the theory and applications of the MIME have been presented elsewhere.[11] Here we present a brief discussion of the theory as it applies to $K_2[PtCl_4]$.

The MIME is best understood in terms of Heller's time-dependent theory of electronic spectroscopy.[13,14] A molecular

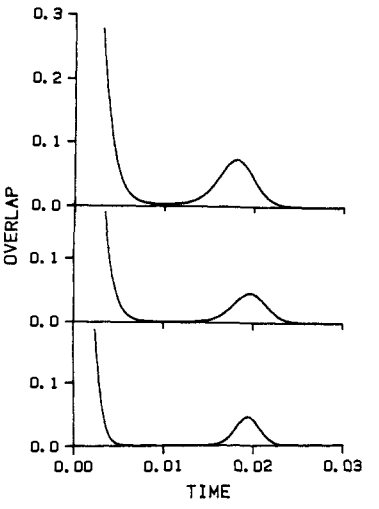

Figure 3. Time dependence of the overlap for the best fit in Figure 2a. Top: 329-cm^{-1} component only. Middle: 304-cm^{-1} component only. Bottom: net time dependence of the overlap; frequency is 315 cm^{-1}. For all plots, Γ = 87 cm^{-1}.

emission spectrum is the Fourier transform of the time-domain overlap of the initial wavepacket (at $t = t_0$) with wavepacket at $t > t_0$. This process starts with a wavepacket whose wave function ϕ_k is an eigenfunction of the lowest vibrational level in the first excited state potential surface. This packet is projected vertically (i.e., with no initial bond length changes) onto the ground state potential surface whose minimum is displaced along the A_{1g} and B_{1g} normal coordinates. The projected wavepacket is not a stationary state of the ground state potential surface. The wavepacket will propagate on the potential surface with the period of the normal mode, and the overlap of the wave function $\phi_k(t)$ propagated wavepacket with ϕ_k of the initial wavepacket will recur with this periodicity. Relaxation into other modes or into the thermal bath causes subsequent recurrences of the overlap to decrease in magnitude. The relaxation is expressed mathematically by multiplying the overlap function by a Gaussian damping factor. The damped overlap function is written as[11]

$$|\langle\phi_k|\phi_k(t)\rangle| = \exp[-(1/2)\Delta_k^2(1 - \cos\omega_k t) - \Gamma^2 t^2] \quad (1)$$

where Δ_k is the equilibrium distortion of the first excited k state in the k^{th} normal mode. Because the potential surfaces are displaced in more than one normal mode, the total overlap will be the product of the overlap functions for each normal mode, $\Pi\langle\phi_k|\phi_k(t)\rangle$. The emission spectrum is the Fourier transform of the time-domain function[11]

$$I(\omega) = C\omega^3 \int_{-\infty}^{\infty} e^{i\omega t}\{\Pi\langle\phi_k|\phi_k(t)\rangle\}\, dt \quad (2)$$

where C is a constant and ω is the frequency in the emission spectrum. The procedure for obtaining the theoretical absorption spectrum is identical, except the roles of the upper and lower potential surfaces are reversed, and there is a prefactor of ω instead of ω^3 in the frequency-domain expression. In the limit where each mode can be expressed as a simple harmonic oscillator function, the time-dependent theoretical calculation and the calculation based on the Franck-Condon factors are identical.

The origin of the MIME in $K_2[PtCl_4]$ can be understood by considering the time-domain process which gives rise to the frequency-domain emission spectrum. In the case of $K_2[PtCl_4]$, the normal vibrational modes which play a role have frequencies of 304 cm^{-1} (B_{1g}) and 329 cm^{-1} (A_{1g}). Under the assumption of harmonic modes displaced by ΔB_{1g} and ΔA_{1g}, respectively, but otherwise the same in both electronic states, the total overlap $\langle\phi|\phi(t)\rangle$ factors into two overlaps, one for each mode:

$$\langle\phi|\phi(t)\rangle = \langle\phi_{304}|\phi_{304}(t)\rangle\langle\phi_{329}|\phi_{329}(t)\rangle \quad (3)$$

(12) Hiraishi, J.; Shimanouchi, T. *Spectrochim. Acta* **1966**, *22*, 1483.

(13) Heller, E. J. *J. Chem. Phys.* **1975**, *62*, 1544.

(14) Heller, E. J. *Acc. Chem. Res.* **1981**, *13*, 368.

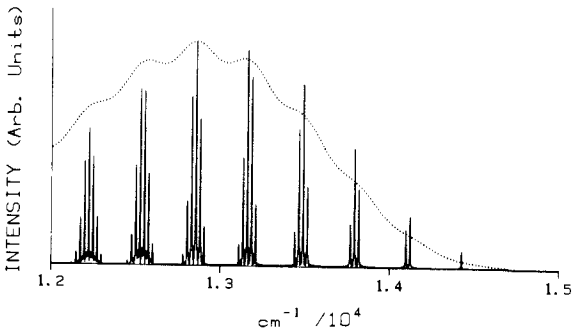

Figure 4. Effect of Γ on the calculated emission spectrum for $K_2[PtCl_4]$: (—), Γ = 1 cm^{-1}; (···), Γ = 100 cm^{-1}. The other calculation parameters are the same as those in Figure 2a.

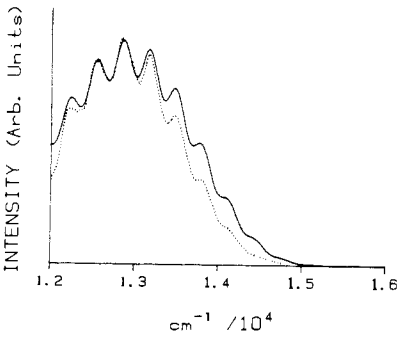

Figure 5. Experimental (···) and calculated (—) emission spectra of $K_2[PtCl_4]$. The calculated spectrum is the best fit obtainable by placing E_{00} in the middle of the energy gap. Experimental conditions: single crystal, 10 K, E||c polarization. Calculation parameters: two modes: A_{1g}, 239 cm^{-1}, Δ = 2.61; B_{1g}, 304 cm^{-1}, Δ = 2.99, E_{00} = 15055 cm^{-1}, Γ = 87 cm^{-1}.

The evolution of these overlaps is shown in Figure 3. In each case, an initial decay is followed by a recurrence that is caused by the return of the moving wavepacket to its starting position. For the B_{1g} mode (Figure 3a) the recurrence peaks at $t_1 = 2\pi/(304\ cm^{-1})$, while for the A_{1g} mode (Figure 3b) the recurrence is at $t_2 = 2\pi/(329\ cm^{-1})$. The product of the time-domain functions (Figure 3c) has its recurrence at $t_M = 2\pi/(315\ cm^{-1})$. The partial recurrence at $2\pi/(315\ cm^{-1})$ is responsible for the appearance of a regularly spaced progression in the emission spectrum at a frequency of 315 cm^{-1}. Note that this compromise recurrence time t_M is not just the arithmetical average of t_1 and t_2. If one changes ΔB_{1g} and ΔA_{1g} relative to each other, the value of t_M (and ω_M) can be tuned over large ranges, i.e., the MIME frequency need not bear any simple relationship to the normal-mode frequencies.

A requirement for the appearance of the MIME is that the spectrum must not be fully resolved, i.e., the damping factor Γ must be large. The effect of Γ on the spectrum in the frequency domain is illustrated in Figure 4 for the example of $K_2[PtCl_4]$. If the damping is small, for example, Γ = 1 cm^{-1}, then there will be many recurrences of the overlap in the time domain and the emission spectrum will exhibit sharp, well-resolved lines. In the limit of small damping, no MIME frequency will be observed. Instead, progressions in each of the normal modes and combination bands will be observed. If the damping is increased (to 100 cm^{-1}, for example) the recurrences at long times will be damped out and disappear giving a spectrum that is less fully resolved. The MIME effect can occur under these conditions. Each vibronic peak in the emission spectrum consists of various contributions from the normal modes and their combinations. Even in the simple example shown in Figure 4, no simple relationship between an observed vibronic peak and the normal modes contributing to it is apparent. For example, the major contributors to the sixth peak in the poorly resolved spectrum are unequally weighted combination bands. The major contributor consists of three quanta of ω_1 and two quanta of the ω_2. The minor contributors consist of two quanta of ω_1 and three quanta of ω_2, and of four quanta of ω_1 and one quantum of ω_2. When the damping is extremely large, there will be no recurrences of the overlap in the time domain and the emission spectrum will consist only of a broad envelope.

A simplified expression which gives an estimate of the MIME frequency is[15] $\omega_M = \{\sum_k \omega_k^2 \Delta_k^2 + 4\Gamma^2\}/\sum_k \omega_k \Delta_k^2 \eta_k$, where η_k is an integer which corresponds to the number of return visits in the kth mode when all the contributing modes are closest to recurring, and the other symbols are as previously defined. The values of η_k are equal to one for both the A_{1g} and B_{1g} modes. One can see from this expression how the MIME frequency ω_M can be tuned between the 304- and 329-cm^{-1} frequencies by changing the relative distortions (Δ_k) in each mode. The MIME frequency in the emission spectrum of $K_2[PtCl_4]$, estimated by using the simple formula and the parameters from the fit in Figure 2a, is 322 cm^{-1}.

2. Excited-State Geometry of $PtCl_4^{2-}$. The normal coordinate equilibrium displacement determined by the fit can readily be expressed in terms of bond length changes in Å. Only the magnitudes are determined. For the d–d transition to the σ antibonding $d_{x^2-y^2}$ orbital it is logical to assume that the equilibrium A_{1g} displacement corresponds to bond lengthening. The relationships between the normal coordinate Δ and the Pt–Cl bond length changes δ(Pt–Cl) are

$$\Delta A_{1g} = (1/2)[\delta(\text{Pt–Cl})_1 + \delta(\text{Pt–Cl})_2 + \delta(\text{Pt–Cl})_3 + \delta(\text{Pt–Cl})_4] \quad (4)$$

$$\Delta B_{1g} = (1/2)[\delta(\text{Pt–Cl})_1 - \delta(\text{Pt–Cl})_2 + \delta(\text{Pt–Cl})_3 - \delta(\text{Pt–Cl})_4] \quad (5)$$

When Δ is converted from dimensionless normal coordinates used in eq 1 to δ(Pt–Cl) in Å units, the increase in the length of each Pt–Cl bond from the totally symmetric distortion is 0.06 Å.[16] In the B_{1g} direction, one pair of chloride ligands opposite to each other are elongated by 0.06 Å while the other pair is contracted by the same amount. The net result is that the molecule has a D_{2h} excited-state symmetry in which the square plane has changed to a rhombus.

The emission occurs from the D_{2h} molecule. In this point group, the normal mode which had B_{1g} symmetry in D_{4h} now has A_{1g} symmetry. The progression in this mode is allowed. The Γ_1 excited state retains Γ_1 symmetry in D_{2h}. Thus, an electric dipole transition requires one quantum of B_{1u}, B_{2u}, or B_{3u} excitation as the promoting mode.

3. The Energy Gap. The energy gap in the spectra of $K_2[PtCl_4]$ is the region between the emission spectrum and absorption spectrum extending between 14435 and 16200 cm^{-1} in which both spectra are flat to the baseline (Figure 1). Usually, the emission and absorption spectra overlap at the E_{00} band. Crystal defects may shift the emission band to slighly lower energy, but such shifts are usually much smaller than the 1800-cm^{-1} gap observed here. Careful examination of very thick crystals revealed no absorption bands in this region. This observation is consistent with the earlier work of Patterson et al.[3] Vanquickenborne and Ceulemans have made the observation that spin–orbit coupling in $K_2[PtCl_4]$ should lend considerably intensity to the spin- and LaPorte-forbidden transitions and that therefore no "hidden" bands should be present in this complex below 16200 cm^{-1}.[6] A careful search for emission in the gap did not reveal any bands to high energy of the 14435-cm^{-1} peak which is assigned as the E_{00} band.

The simplest explanation of the energy gap is that the optical transition probabilities in this region are small because of very large distortions of the molecule between the ground and excited electronic states. According to this explanation, the 0–0 transitions

(15) Tutt, L.; Zink, J. I.; Heller, E. J. *Inorg. Chem.* **1987**, *26*, 2158.

(16) To convert from dimensionless units to Å, one uses the following formulas: $D = (h/4\pi^2 c\omega\mu)^{1/2} \times \Delta \times 10^8$ Å/cm, where, D is the distortion in the normal coordinate in Å, Δ is the distortion in the normal coordinate in dimensionless units, h = Planck's constant in g cm^{-} s^{-1}, c = the speed of light in cm s^{-1}, ω = the frequency of the mode in cm^{-1}, and μ = the reduced mass for the mode in g ($\mu_{A1g} = 5.89 \times 10^{-23}$ g.)

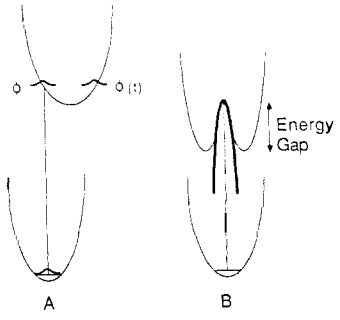

Figure 6. Potential energy surface for a totally symmetric mode (A) and a non-totally symmetric mode (B).

of both the emission and absorption spectra would be near the middle of the energy gap. This idea has been used to explain the energy gap in the spectrum of $K_3[Co(CN)_6]$.[17] In order to test this explanation for $K_2[PtCl_4]$ a series of emission spectra were calculated by using the methods described above with the value of E_{00} ranging from 14 110 to 15 055 cm^{-1}. The calculation with E_{00} = 15 055 cm^{-1}, i.e., near the middle of the energy gap, and large distortions in the A_{1g} and B_{1g} modes is shown in Figure 5. As required, the intensities at the high energy end of the emission spectrum are low because the Franck-Condon factors are small. However, it is impossible to obtain a good fit to the spectrum. In Figure 5, the intensities of only a few of the vibronic bands can be made to fit the experimental spectrum. Thus, large distortions and a spectral origin in the middle of the energy gap cannot account for the experimental spectrum.

The cause of the spectral energy gap in $K_2[PtCl_4]$ can be understood by considering the excited-state potential surfaces for the symmetric as well as the non-totally symmetric modes. These surfaces will resemble the cross-sections shown in Figure 6. The abcissa in this figure is the bond length $Q(k)$ along the normal coordinate k. In the case of $K_2[PtCl_4]$, the right side of Figure 5 represents a slice through the B_{1g} normal mode at $Q(A_{1g})$ = ΔA_{1g} = 2.58, and the left side represents a slice through the A_{1g} normal mode at $Q(B_{1g})$ = 0. In the absorption process, the wavepacket starts out at the minimum of the lower surface, then it moves vertically to the upper surface. At time t = 0 it begins to propagate on the upper surface. It moves rapidly down the steep slope in the A_{1g} direction and spreads in the B_{1g} direction. If the spreading in the B_{1g} direction is slow, there is little propagation of the wavepacket on the lowest portions of the potential surface. Consequently, there will be a region of the upper potential surface (indicated by "energy gap" in Figure 6) which the wavepacket will explore little or not at all. The absorption spectrum will not contain information about this low-energy region giving rise to the energy gap in the absorption spectrum.

Two simple calculations support this model. First, the magnitude of the energy gap is calculated from the magnitude of the distortion in the B_{1g} direction which is obtained from analysis of the emission spectrum. Second, the effects of wavepacket spreading on the magnitude of the intensities in the energy gap are calculated by using a simple model of the potential.

Magnitude of the Energy Gap. To obtain an estimate of the energy gap to test the model, each half of the upper potential surface in the right side of Figure 6 is approximated as a harmonic oscillator. The energy of the gap, which should be roughly the energy difference between the saddle point and the energy minimum of the upper surface, can be estimated as E_{eg} = $(1/2)\omega_0\Delta B_{1g}^2$, where ω_0 is the frequency of the non-totally symmetric mode and ΔB_{1g} is the excited-state distortion in the non-totally symmetric mode. Using the values for the B_{1g} mode obtained from the fit to the experimental emission spectrum (ω_0 = 304 cm^{-1}, ΔB_{1g} = 2.58), the energy gap is calculated to be 1012 cm^{-1}. This calculation provides a good order of magnitude estimate of the gap in the spectrum of $K_2[PtCl_4]$ considering the simplicity of the model being used.

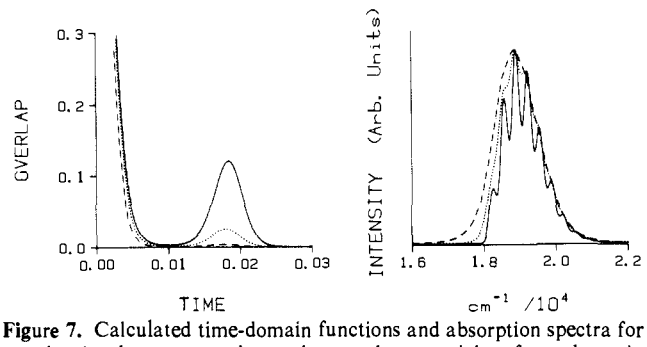

Figure 7. Calculated time-domain functions and absorption spectra for a molecule whose wavepacket evolves on the potential surfaces shown in Figure 5. Right: absorption spectra for a steep inversion (ω = 300 cm^{-1}, dashed line), a broad inversion (ω = 100 cm^{-1}, solid line), and one intermediate between these (ω = 200 cm^{-1}, dotted line). Left: the corresponding plots of the magnitude of the overlap versus time.

Low Intensities in the Energy Gap. A very simple model of a potential surface for the non-totally symmetric mode which leads to wavepacket spreading and which gives an expression for the intensities in closed form is the "inverted harmonic oscillator" surface given by $V = -1/2\omega Q^2$. For small values of Q, this surface is used as a model of the potential surface in the region of the ground-state internuclear geometry as shown in Figure 6 by the surface drawn in bold face. The time dependence of the overlap of a wavepacket spreading on such a surface has been derived by Heller

$$\langle\phi_k|\phi_k'(t)\rangle = \{2[2\cosh\omega t - i(\omega/\omega_0)\sinh\omega t + i(\omega_0/\omega)\sinh\omega t]\}^{-1/2} \quad (6)$$

where ω_0 is the frequency of the non-totally symmetric mode in the ground state, and ω is the frequency of the inverted potential in the excited state. In calculating the absorption spectrum, the expression above is used in place of the expression in eq 1 for each *non*-totally symmetric mode distortion.

Model calculations on a system with one totally symmetric mode and one non-totally symmetric mode show that the intensity in the energy gap is low. Three calculated absorption spectra using three different values of ω for the inverted harmonic are shown in the right side of Figure 7. The broader the inverted surface, the slower the spreading of the wavepacket and the smaller the energy region of the inverted surface which is explored. Consequently, the absorption spectrum (solid line) has very low intensity on the low-energy side. The steeper the inverted surface, the faster the spreading of the wavepacket, and the larger the energy region of the inverted surface which is explored. The spectral consequence is increasing intensity in the low-energy region of the spectrum (dotted line, dashed line).

Note also that a steeper inverted potential results in less vibronic structure on the absorption band. If the inverted potential is broad, the wavepacket will not have spread much in the non-totally symetric direction before recurrences take place in the totally symmetric direction (Figure 7, left side). The resulting absorption spectrum has vibronic structure whose frequency is that of the totally symmetric mode. If the inverted potential has a steep slope, the wavepacket will spread before it can recur in the totally symmetric direction, and the absorption spectrum will be featureless.

In general, a significant excited-state distortion in a non-totally symmetric mode may result in the presence of an energy gap. Conversely, when the excited state is distorted in only one or more totally symmetric modes, there should be no apparent gap between the emission and absorption spectra. An example of the latter case may be seen in the polarized single-crystal low-temperature electronic spectra of the closely related complex, $[PtBr_4]^{2-}$. The emission spectrum has a well-resolved vibronic structure whose spacing is 205 cm^{-1}. The frequency of the only totally symmetric mode in this complex is also 205 cm^{-1}. Thus the emission spectrum can be fit by using a distortion in only the totally symmetric mode,

(17) Miskowski, V. M.; Gray, H. B.; Wilson, R. B.; Solomon, E. I. *Inorg. Chem.* **1979**, *18*, 1410.
(18) Heller, E. J., private communication.

and no energy gap should be present. Experimentally, no energy gap is found. The E_{00} band of the emission spectrum is at about 13 850 cm^{-1}; the absorption spectrum has its initial intensity at about 14 000 cm^{-1}.[4,5,19]

It has been shown that the energy gap and the vibronic spacing in the electronic spectra of the $[PtCl_4]^{2-}$ ion are explained by an excited-state distortion in a non-totally symmetric mode. The 315-cm^{-1} MIME frequency results from the distortion in the 329-cm^{-1} A_{1g} mode and the 304-cm^{-1} B_{1g} mode. The low intensity in the energy gap is a result of slow wavepacket spreading along the B_{1g} coordinate.

Acknowledgment. The support of the National Science Foundation (CHE85-09329) (J.I.Z. and D.M.P.) and of the Deutsche Forschungsgemeinschaft (G.G. and A.L.) is gratefully acknowledged. The authors thank Professor E. J. Heller of the University of Washington in Seattle for the derivation of eq 6 and also thank Kyeong-Sook Shin for helpful discussions and for producing Figure 7.

Registry No. $K_2[PtCl_4]$, 10025-99-7.

(19) Kroenig, R. F.; Rush, R. M.; Martin, D. S.; Clardy, J. C. *Inorg. Chem.* **1974**, *13*, 1366.

Gas-Phase Heats of Formation of $C_7H_7^+$ Isomers: *m*-Tolyl, *p*-Tolyl, and Benzyl Ions

Tomas Baer,* J. C. Morrow, Jian Dong Shao, and Susan Olesik[†]

Contribution from the Department of Chemistry, University of North Carolina, Chapel Hill, North Carolina 27599-3290. *Received February 16, 1988*

Abstract: The dissociation onsets of $C_7H_7^+$ formation from the ionic precursors of benzyl bromide and *m*- and *p*-nitrotoluene have been investigated by photoelectron photoion coincidence in order to determine accurate heats of formation of the resulting $C_7H_7^+$ ion structures. These parent ions are known to produce 100% benzyl and tolyl ions, respectively. Because the benzyl bromide ion dissociation was found to be rapid, the dissociation onset was determined from the crossover energy in the breakdown diagram and appropriately corrected for the precursor thermal energy. The nitrobenzene ions dissociate slowly near the dissociation onset, so that the thermochemical onset was found by extrapolating the measured decay rates with the RRKM/QET statistical theory. The rate data indicate that *p*- and *m*-nitrotoluene ions do not isomerize to a common structure prior to dissociation. This suggests that the *p*- and *m*-tolyl ions also exist as unique structures. However, no information about the *o*-tolyl ion was obtained. The derived ionic heats of formation were $\Delta H_f°_{298}$(*m*-tolyl) = 1054 ± 10 kJ/mol, $\Delta H_f°_{298}$(*p*-tolyl) = 1074 ± 10 kJ/mol, and $\Delta H_f°_{298}$(benzyl) = 897 ± 5 kJ/mol. An upper limit for the heat of formation of $C_6H_4CH_3O^+$, the NO loss product from the *p*-nitrotoluene ion, was determined to be 890 kJ/mol. These heats of formation allow the methyl and ring C–H bond energies in the toluene ion to be calculated. They are 2.18 and 3.9 eV, respectively.

I. Introduction

The structures and energies of the $C_7H_7^+$ ions have fascinated chemists ever since the discovery by Doering and Knox[1] that the seven-membered cyclic structure known as the tropylium ion is stable in solution and that cycloheptatrienyl bromide appears to be ionized in the solid form.[2] The origin of this stability has been attributed to aromaticity, in which cyclic compounds with $4n + 2$ (n = 1–3, etc.) electrons are particularly stable. The tropylium ion has six π electrons, similar to the benzene molecule. In addition to the tropylium ion, there are many other possible structures of $C_7H_7^+$. Among the most stable are the benzyl and tolyl ions.

Investigations of gas-phase $C_7H_7^+$ ions have been carried out for a number of years by a variety of techniques including mass spectrometry,[3-7] collisional activation (CA),[8-13] ion cyclotron resonance (ICR),[14-17] photoionization (PI),[18-22] and photoelectron photoion coincidence (PEPICO),[23] as well as by molecular orbital calculations.[24,25] These studies show that there are three primary $C_7H_7^+$ structures that are produced in the dissociative ionization of various precursor molecules. These are, in order of increasing energy, the tropylium (I), the benzyl (II), and the tolyl (III) ions.

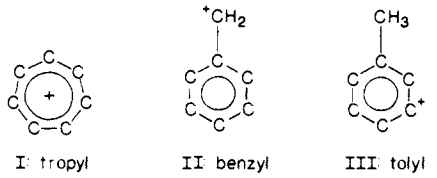

I: tropyl II: benzyl III: tolyl

Ion III has three different isomers, which differ in the position of the charge site on the ring relative to the methyl group. There

[†] Present address: Chemistry Department, The Ohio State University, Columbus, OH 43210.

(1) Doering, W. v. E.; Knox, L. H. *J. Am. Chem. Soc.* **1954**, *76*, 3203.
(2) Hine, J. *Physical Organic Chemistry*; McGraw-Hill: New York, 1962; p 27.
(3) Brown, P. *J. Am. Chem. Soc.* **1968**, *90*, 4461.
(4) Yeo, A. N. H.; Williams, D. H. *J. Chem. Soc., Chem. Commun.* **1970**, 886.
(5) Stapleton, B. J.; Bowen, R. D.; Williams, D. H. *J. Chem. Soc., Perkin Trans. 2* **1979**, 1219.
(6) Tajima, S.; Tsuchiya, T. *Org. Mass Spectrom.* **1974**, *9*, 265.
(7) Leung, H. W.; Ichikawa, H.; Li, Y. H.; Harrison, A. G. *J. Am. Chem. Soc.* **1978**, *100*, 2479.
(8) McLafferty, F. W.; Winkler, J. *J. Am. Chem. Soc.* **1974**, *96*, 5182.
(9) McLafferty, F. W.; Bockhoff, F. M. *Org. Mass Spectrom.* **1979**, *14*, 181.
(10) Dymerski, P. P.; McLafferty, F. W. *J. Am. Chem. Soc.* **1976**, *98*, 6070.
(11) McLafferty, F. W.; Proctor, C. J. *Org. Mass Spectrom.* **1983**, *18*, 193.
(12) Buschek, J. M.; Ridal, J. J.; Holmes, J. L. *Org. Mass Spectrom.*, in press.
(13) Olesik, S.; Baer, T.; Ridal, J. J.; Buschek, J. M.; Holmes, J. L.; Morrow, J. C., to be submitted for publication in *Org. Mass Spectrom.*
(14) Jackson, J. A. A.; Lias, S. G.; Ausloos, P. *J. Am. Chem. Soc.* **1977**, *99*, 7515.
(15) Dunbar, R. C. *J. Am. Chem. Soc.* **1975**, *97*, 1382.
(16) Honovich, J. P.; Dunbar, R. C. *Int. J. Mass Spectrom. Ion Processes* **1982**, *42*, 33.
(17) Fu, E. W.; Dymerski, P. P.; Dunbar, R. C. *J. Am. Chem. Soc.* **1976**, *98*, 337.
(18) Akopyan, M. E.; Vilesov, F. K. *Russ. J. Phys. Chem.* **1966**, *40*, 63.
(19) McLoughlin, R. G.; Morrison, J. D.; Traeger, J. C. *Org. Mass Spectrom.* **1979**, *14*, 104.
(20) McLoughlin, R. G.; Morrison, J. D.; Traeger, J. C. *Org. Mass Spectrom.* **1978**, *13*, 483.
(21) Traeger, J. C.; McLoughlin, R. G. *J. Am. Chem. Soc.* **1977**, *99*, 7351.
(22) Lifshitz, C.; Goldenberg, M.; Malinovich, Y.; Peres, M. *Org. Mass Spectrom.* **1982**, *17*, 453.

0002-7863/88/1510-5633$01.50/0